

COMPLEMENTARY AES AND AEM OF GRAIN BOUNDARY REGIONS
IN IRRADIATED γ' -STRENGTHENED ALLOYS*

DE86 010397

K. Farrell, N. Kishimoto[†], R. E. Clausing, L. Heatherly, and G. L. Lehman[#]Metals and Ceramics Division, Oak Ridge National Laboratory
P. O. Box X, Oak Ridge, TN 37831 (USA)[†]National Research Institute for Metals, Tsukuba Laboratories
Sakara-Mura, Ibaraki 305, Japan[#]Formerly with Oak Ridge Associated Universities, Oak Ridge, TN 37831;
Present address: JEOL, USA, Inc., 11 Dearborn Road,
Peabody, MA 01960 (USA)

ABSTRACT.

Two microchemical analysis techniques are used to measure solute segregation at grain boundaries in two γ' -strengthened, fcc Fe-Ni-Cr alloys that display radiation-induced intergranular fracture. Scanning Auger electron spectroscopy (AES) of grain boundary fracture surfaces and analytical electron microscopy (AEM) of intact grain boundaries using energy-dispersive x-ray spectroscopy show good agreement on the nature and extent of segregation. The elements Ni, Si, Ti, and Mo are found to accumulate in α , Laves and γ' phases on the grain boundaries. Segregation of P is detected by AES. The complementary features of the two analytical techniques are discussed briefly.

MASTER

*Research sponsored by the Division of Materials Sciences, U.S. Department of Energy, under contract DE-AC05-84OR21400 with Martin Marietta Energy Systems, Inc.

DISCLAIMER

This report was prepared as an account of work sponsored by an agency of the United States Government. Neither the United States Government nor any agency thereof, nor any of their employees, makes any warranty, express or implied, or assumes any legal liability or responsibility for the accuracy, completeness, or usefulness of any information, apparatus, product, or process disclosed, or represents that its use would not infringe privately owned rights. Reference herein to any specific commercial product, process, or service by trade name, trademark, manufacturer, or otherwise does not necessarily constitute or imply its endorsement, recommendation, or favoring by the United States Government or any agency thereof. The views and opinions of authors expressed herein do not necessarily state or reflect those of the United States Government or any agency thereof.

DISTRIBUTION OF THIS DOCUMENT IS UNLIMITED

UNLIMITED

INTRODUCTION

When fcc alloys of the Fe-Ni-Cr system are precipitation-hardened with γ' phase and irradiated and tested at temperatures in the range 500–800°C they tend to display low ductilities and intergranular failure [1–6]. Embrittlement is attributed to brittle phases at the grain boundaries [3–5]. This paper describes the results of some microchemical analyses made on grain boundary regions in such specimens using two different and complementary techniques. The intergranular nature of the fractures allows the application of scanning Auger electron spectroscopy (AES), to the exposed grain boundaries. The other technique is analytical electron microscopy (AEM) of intact grain boundaries in TEM foils using energy-dispersive x-ray spectroscopy (EDXS).

MATERIALS AND TECHNIQUES

Specimens of two experimental alloys, designated D21 and D25, were received from the inventory of the National Cladding/Duct Materials Development Program. Their bulk chemical compositions (Table 1) are somewhat similar, the major differences being that D25 contains more Ni and Mo and less Ti than D21. These alloys are designed to be strengthened by fine precipitates of the γ' phase, Ni_3X , where X is Ti, Al, and Si. Prior to irradiation they were solution-annealed for 0.5 h at 1050°C and air-cooled, after which they were precipitation-hardened by aging at 700°C for 24 h. They were then irradiated in EBR-II to a fast fluence ($E > 0.1$ MeV) of 3×10^{26} n/m² (~15 dpa) at 575° and 625°C. Postirradiation mechanical tests made on these alloys [3,5] reveal severe embrittlement.

Our specimens were small bars, 1-mm square section by 10-mm long, with the mid-regions of the bar reduced to a 1-mm \times 0.5 mm section. These were broken in tension at room temperature or at the irradiation temperature in a special device inside a vacuum chamber attached to a Physical Electronics Industries Model 590 scanning Auger microprobe. Prior to fracture, a chamber pressure of $\sim 10^{-7}$ to 10^{-8} Pa was achieved by baking the chamber and its contents at 150–200°C for 8–10 h. Breaking the specimens in this good vacuum minimizes environmental contamination at the fracture surfaces but does not yield mechanical properties data. In-situ fractographic examination showed that the fracture faces of the D21 alloy specimens were predominantly intergranular at all test temperatures; the D25 alloy failed by mixed transgranular and intergranular modes. AES spectra were collected from the exposed grain boundary facets, first in the as-fractured condition and then after successive removals of the facet surface layers by in-situ argon sputtering. This gave information on concentration versus depth profiles. The depths were estimated from the sputter times using an established sputter rate of ~ 0.02 nm/s. For each specimen, areas of at least 1×10^{-10} m² on at least three different grain boundary facets were probed in this manner, and the data were averaged to obtain a typical concentration-depth profile for each specimen.

Following AES of the specimens, wafers were sliced from their cross-sections with a diamond-edge disk saw and were thinned electrolytically to make TEM specimens. These were studied in a Philips EM400T/FEG electron microscope operating at 100 keV. Microchemical analyses were made in the

STEM mode with a beam spot size of ~5 nm using an EDAX 9100/70 system. At grain boundaries a traverse line was set up normal to the boundary and a series of spot analyses was made automatically at preset length intervals across the boundary region. This technique provided concentration profiles perpendicularly across the boundary, corresponding to the AES concentration-depth data but covering a wide range of distances. Interference signals from radioactive decay of the specimens were compensated by collecting a spectrum from within the perforated hole in the specimen and subtracting the hole spectrum from the specimen spectra.

RESULTS

Microstructures

The microstructures of both alloys for both irradiation temperatures were similar. The grain boundaries were covered with abutting, sometimes overlapping, precipitate particles, forming zones 100–350 nm thick straddling the original grain boundaries. Within the grains there were loops, dislocation tangles and a heterogeneous distribution of angular, often elongated, precipitates seemingly similar to those on the grain boundaries (Fig. 1a). These matrix precipitates ranged in size from about 200 nm to ~1.5 μm (longest dimension) and were identified as G phase (a nickel silicide) and a Laves phase of Fe_2Mo type. There was no distinctive morphological difference between particles of the two phases. EDXS analyses gave compositions of 46 at. % Ni, 20Si, 17Ti, 13Fe, 3Cr, 1Mo for the G phase and 18Ni, 10Si, 3Ti, 37Fe, 12Cr, and 20Mo for the Laves phase. Also

present less conspicuously within the grains were many relatively small (25–150 nm), near spherical, coherent particles of γ' phase. These were seen most sharply under dark-field imaging conditions (Fig. 1b). Their spatial distribution was for the most part uniform but in the D25 alloy stringers of γ' particles were superimposed on the uniform distribution. There was denuding of γ' alongside grain boundaries and grain boundary phases, most apparently in D21 alloy where the denuded widths ranged to about 300 nm on each side of the boundary zone. Some γ' precipitates occurred intermittently along grain boundaries interspersed with the grain boundary phases and sometimes decorating them, but there was no continuous coverage of grain boundaries with γ' as seen in irradiated Nimonic Pe-16 alloy [4]. Small gas bubbles were noted on grain boundaries and at the surfaces of G and Laves phases. Low concentrations of gas bubbles or cavities were randomly dispersed within the grains.

AES and AEM Data

Figure 2 shows the average AES data measured on the intergranular fracture facets of D21 alloy irradiated at 625°C. For easy reference, a bar plot of the alloy's bulk composition is included. To avoid crowding in the 0–10 at. % region in the AES data, some of the curves are displayed in the upper boxes. It is clear that the elements Si, Ti and Ni are significantly segregated at the fracture surface at the expense of Fe and Cr. This segregation declines gradually over a depth of about 250 nm below the original fracture faces. A trace of phosphorus is seen at, and just below, the initial fracture surfaces.

Figure 3 depicts the results of an AEM-EDXS linear trace across phases at a grain boundary in a TEM foil from the same specimen. Here, the white crosses indicate the rest positions of the electron beam, corresponding to the data points in the graphs. The points in the column headed M to the right of the graphs are the results of a square raster of a matrix region free of G and Laves precipitates; agreement of these points with the bulk analyses of the alloy lends credence to the significant deviations from the bulk compositions found in the grain boundary regions. It is seen that the grain boundary phases are enriched in Si, Ti, Ni and are depleted in Fe and Cr. Regions on each side of the grain boundary phases are enriched in Fe and depleted in Ni. The compositions of the phases are very similar to the grain boundary regions measured in AES and to the G phase particles within the grains.

Corresponding AES and AEM data for D25 alloy are presented in Figs. 4 and 5. The AES data (Fig. 4) show segregation of Mo, Si, Ti and P at the intergranular fracture surface. With removal of the surface layers, the P level is unaltered and the Ti level declines initially then settles at a level of about twice the bulk value; Si and Mo increase to many times their bulk values at a depth of about 40 nm then retreat at greater depths. Surface removal was done to a depth of 150 nm. Extrapolation of the data linearly indicates that segregation of the major elements in the analyses should disappear at a depth of ~200 nm. The EDXS traverse across and beyond two overlapping precipitate phases on a grain boundary (Fig. 5)

shows that segregation is confined to the precipitate phases and that the segregated elements are the same as those recognized by AES. No P peaks were discerned in AEM. The concentrations of elements in the broad particle in Fig. 5 are compatible with those measured at depths of 20–100 nm in AES and with the Laves particles analyzed within the grains. The narrow phase in Fig. 5 is partially overlapped by the broader one but it is obviously rich in Si, Ti and Ni and depleted in Fe and Cr, with overall composition consistent with the matrix G phase.

DISCUSSION

This work confirms that considerable segregation of solute elements occurs at grain boundaries in these irradiated D25 and D21 alloys, and it quantifies the levels of segregation. The segregating elements are Si, Ti, Ni, Mo and P, all of which are known to respond strongly to radiation-driven segregation in fcc austenitic alloys [7,8]. The segregated elements are shown to be contained within precipitates of G and Laves phases located on the grain boundaries, together with some γ' particles. It is known that each of these phases can form in unirradiated materials by thermal aging, but G phase is a rarity under such circumstances, and thermally-produced Laves phase is unlikely to contain much Ni and Si. So these phases are considered to be radiation-enhanced or modified, rather than radiation-induced. The two techniques of AES and AEM-EDXS concur on the identities of the elements and their degrees of segregation. They also show satisfactory correspondence in their composition-depth profiles, considering the relative paucity of data for the AEM traverses.

The virtues of using the two analytical techniques in complementary fashion are evident. If AES had been used alone, it would have correctly diagnosed the species and levels of segregants but it would not have recognized that the segregants were incorporated in precipitate phases nor would it have identified the several kinds of precipitates. AEM fills this gap. AEM has the advantages of allowing distinction of second phases and permitting identification of them via EDXS and electron diffraction patterns. A shortcoming of AEM, however, is that each spot-analysis affords only a very highly localized peek at the picture; it analyzes a volume of only about 10^{-23} m^3 which could encompass a grain boundary plane of area no more than $\sim 10^{-15} \text{ m}^2$. Use of this technique to establish the generality of the observations over a large area of grain boundary or many grain boundaries would be tedious and inefficient. In contrast, scanning AES can cover relatively enormous areas of grain boundary. When the results of such an AES survey match the limited AEM data, both in composition and in depth (distance) distribution, as they do in the present work, they verify the ubiquity of the grain boundary phases seen in AEM. In turn, the compositional agreement in the depth profiles by the two techniques removes concern about selective sputtering of species in the AES profiles.

AES offers two other benefits in this work. One is that it reveals the segregation of P, which was not detected in AEM. The 1-2 at. % P seen in D25 alloy is much greater than the expected bulk content of <0.1 at. %. Since AEM-EDXS is capable of distinguishing a level of 1% P, these observations suggest that the P is not segregated uniformly within the grain

boundary phases but probably occurs in discrete phosphide particles, or in thin interfacial films, that were not intercepted by the limited AEM spot probes. The other benefit of AES is that it is more sensitive to carbon than is conventional AEM-EDXS. Often, this high sensitivity cannot be used to advantage because of interference from adventitious carbon (and oxygen) films which are adsorbed readily on to fresh metal surfaces from the atmosphere. The problem of such contamination is usually handled by deleting carbon and oxygen peaks from the Auger data before normalizing the balance of the elements to 100% total. This, of course, denies any conclusion regarding the presence of carbon or carbide phases within the surface regions. In the present work, care was taken to minimize atmospheric contamination by producing and maintaining the fracture surface in UHV conditions. While this did not totally eliminate C and O contamination, it reduced contamination to the point where the characteristic shapes of Auger peaks due to carbides should have been distinguishable from those due to other forms of carbon. No carbide peaks were detected. From this we can conclude that there are little or no carbide phases in the grain boundary regions. This is consistent with the AEM findings that the grain boundary phases are primarily intermetallic compounds and silicides.

Others [3,5] have studied the general microstructure and grain boundary regions in neutron irradiated specimens of these alloys using TEM and AEM-EDXS without the backing of AES of intergranular fracture surface. In many respects, the earlier findings are similar but less detailed than

those described herein. Segregation of P was not recorded but the phases G, Laves and γ' are reported on the grain boundaries; additionally, a relatively coarse, fern-like precipitate of MC decorated the grain boundaries of the solution-treated-and-aged D25 alloy [5]. These MC ferns were especially evident in carbon extraction replicas. We have not seen this phase in our TEM foils, perhaps because it may not be uniformly-dispersed on the boundaries. We have begun some extraction work on discarded TEM foils and our first attempts have revealed some fern-like impressions in the replicas, but the source of the impressions evaded extraction. Work is continuing, with the goal of understanding intergranular embrittlement in these alloys. Such embrittlement will be the subject of a future paper.

ACKNOWLEDGMENTS

N. H. Rouse deserves credit for his assistance with the experimental work, Mrs. W. E. Gilliam for secretarial services, Drs. E. A. Kenik and J. Bentley for technical advice, Dr. A. F. Rowcliffe for providing the specimens, and Dr. L. K. Mansur for constant encouragement.

REFERENCES

1. A. F. Rowcliffe and J. A. Horak, Trans ANS 38 (1981) 266.
2. R. Bajaj, R. P. Shogan, C. DeFlicht, R. L. Fish, M. M. Paxton, and M. L. Bleiberg, in Effects of Radiation on Materials: Tenth Conference, ASTM STP 725, Eds. D. Kramer, et al. (Amer. Soc. for Testing and Materials, 1981) p. 326.
3. S. Vaidyanathan, T Lauritzen and W. L. Bell, in Effects of Radiation on Materials: Eleventh Conference, ASTM STP 722, Eds., H. R. Brager and J. S. Perrin (Amer. Soc. for Testing and Materials, 1982) p. 619.
4. W. J. S. Yang, J. Nucl. Mater. 108&109 (1982) 339.
5. W. J. S. Yang, D. S. Gelles, J. L. Straalsund, and R. Bajaj, J. Nucl. Mater. 132 (1985) 249.
6. F-H. Huang and R. L. Fish, in Effects of Radiation on Materials: Twelfth International Symposium, ASTM STP 870, Eds., F. A. Garner and J. S. Perrin (Amer. Soc. for Testing and Materials, 1985) p. 720.
7. E. H. Lee, P. J. Maziasz and A. F. Rowcliffe, in Phase Stability During Irradiation, Eds. J. R. Holland, et al., (Met. Soc. AIME, 1981), p. 191.
8. W. J. S. Yang, H. R. Brager and F. A. Garner, in Phase Stability During Irradiation, Eds. J. R. Holland, et al., (Met. Soc. AIME, 1981), p. 257.

Table 1. Bulk chemical compositions of the alloys

		<u>Fe</u>	<u>Ni</u>	<u>Cr</u>	<u>Ti</u>	<u>Al</u>	<u>Si</u>	<u>Mn</u>	<u>Mo</u>	<u>Zr</u>	<u>B</u>	<u>C</u>
D21	wt %	59.3	24.5	8.2	3.4	1.6	1.0	1.0	1.0	--	0.006	0.051
	at. %	56.6	23.4	8.9	4.0	3.3	1.9	1.0	0.6	--	0.031	0.24
D25	wt %	51.8	29.4	10.4	1.8	1.3	0.9	1.0	3.3	0.005	0.006	0.05
	at. %	50.1	28.5	11.4	2.1	2.8	1.8	1.0	2.0	0.003	0.031	0.24

FIGURE CAPTIONS

Fig. 1. Examples of microstructural features. (a) D25 alloy irradiated at 575°C, showing grain boundary regions, dislocations and large matrix precipitates. (b) γ' precipitates revealed under dark-field conditions.

Fig. 2. D21 Alloy. Bulk composition and AES analyses of intergranular fracture surfaces. For clarity in the 0-10 at. % region, the data for Al, Si and Ti are shown separately.

Fig. 3. D21 Alloy. Compositions obtained during an AEM traverse across precipitate phases on a grain boundary.

Fig. 4. D25 Alloy. Bulk composition and AES analyses of intergranular fracture surfaces.

Fig. 5. D25 Alloy. AEM composition data measured across precipitate phases on a grain boundary.

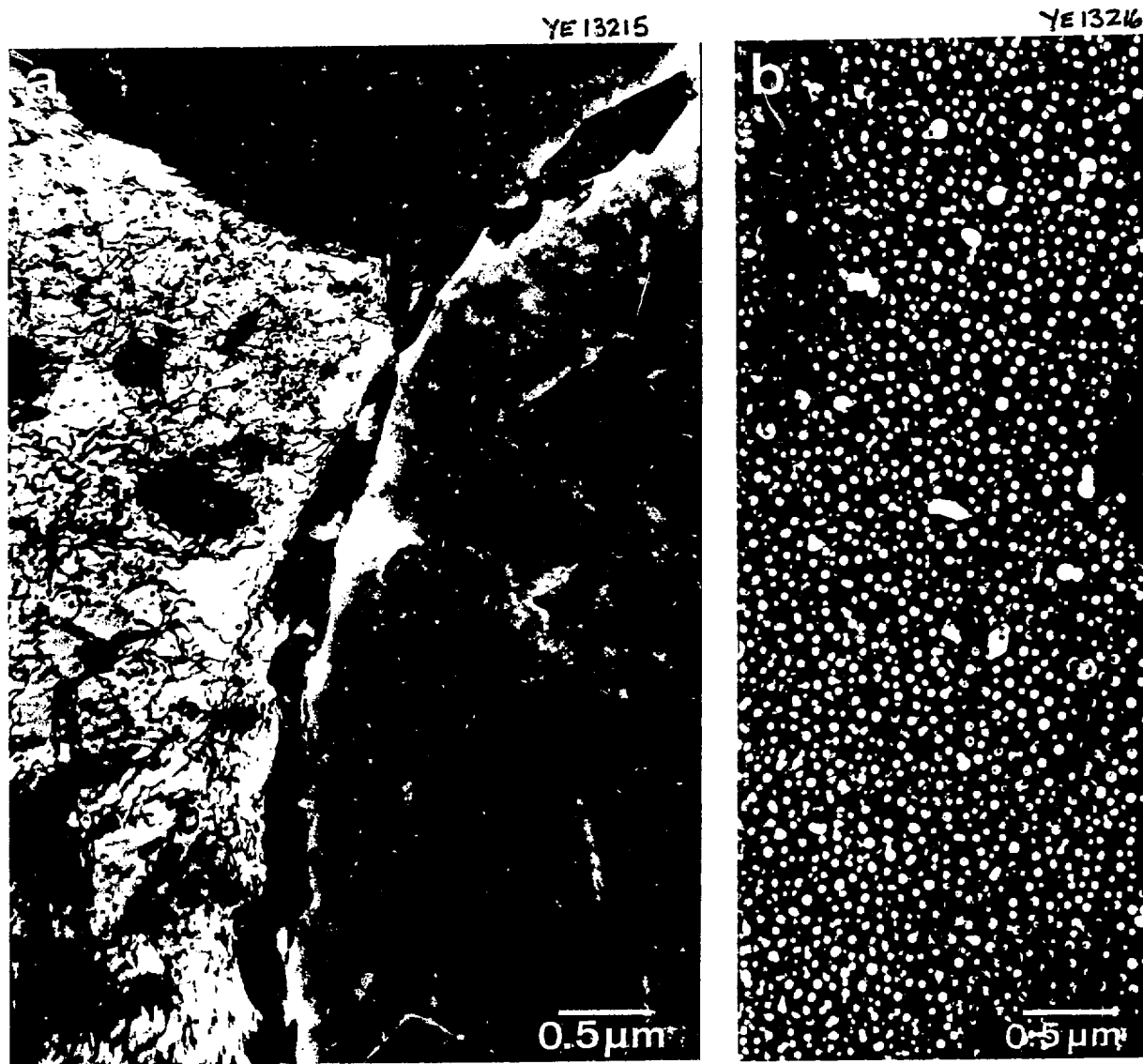


Fig. 1. Examples of microstructural features. (a) D25 alloy irradiated at 575°C, showing grain boundary regions, dislocations and large matrix precipitates. (b) γ' precipitates revealed under dark-field conditions.

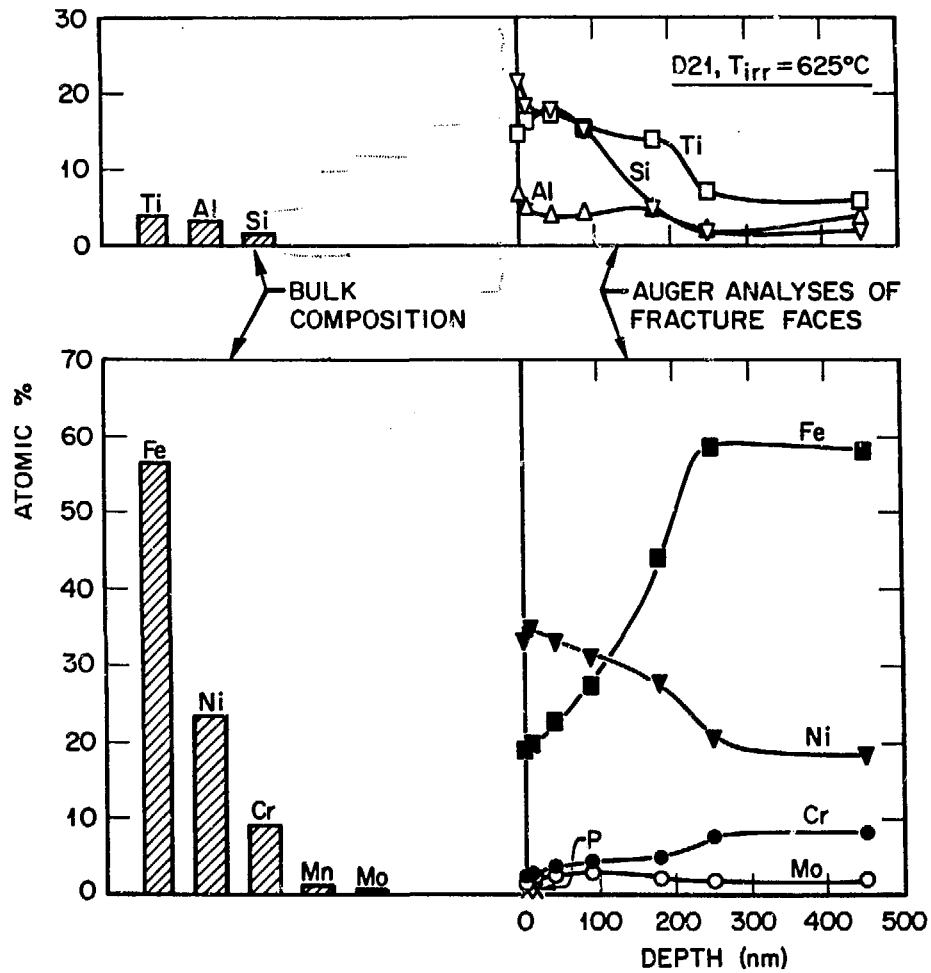


Fig. 2. D21 Alloy. Bulk composition and AES analyses of intergranular fracture surfaces. For clarity in the 0-10 at. % region, the data for Al, Si and Ti are shown separately.

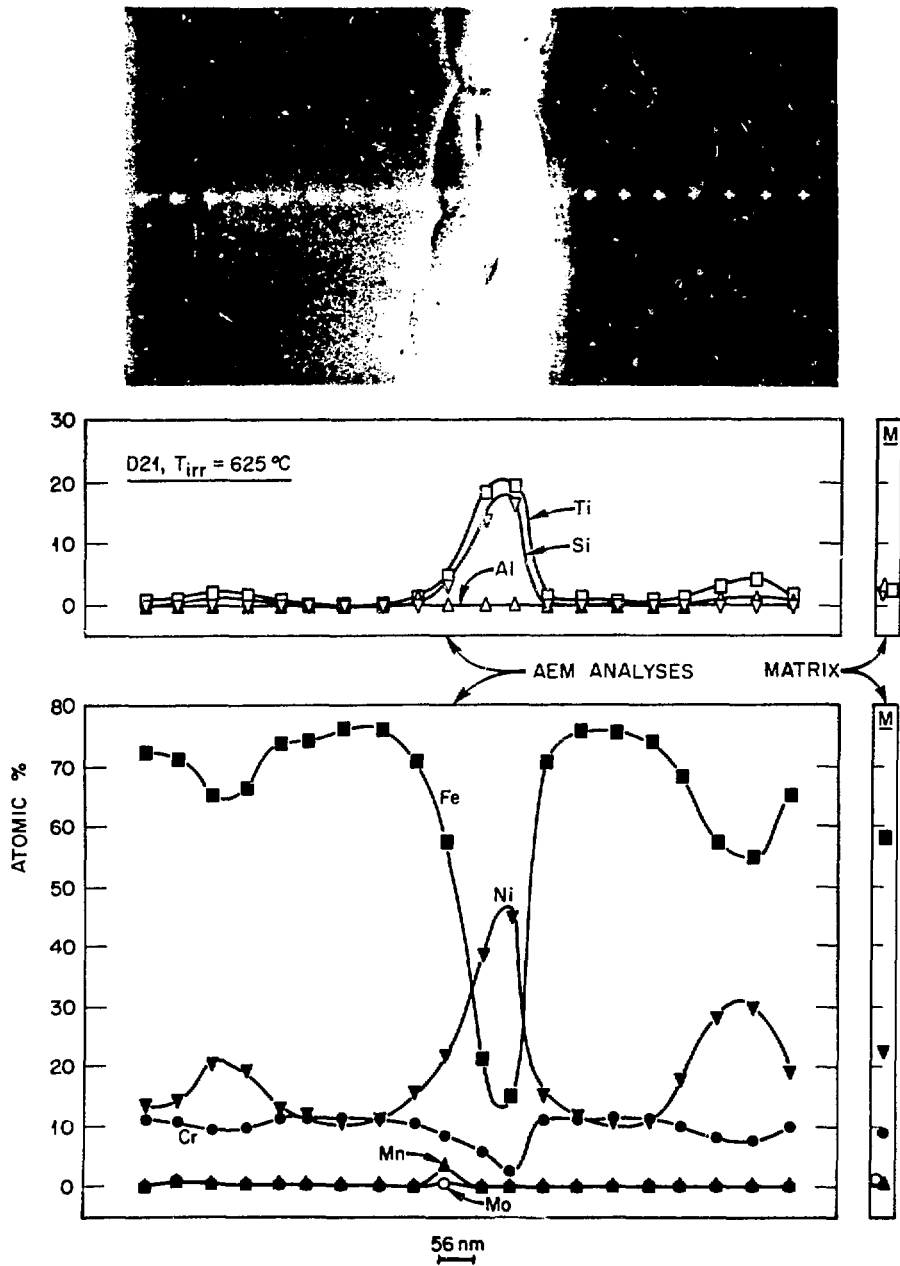


Fig. 3. D21 Alloy. Compositions obtained during an AEM traverse across precipitate phases on a grain boundary.

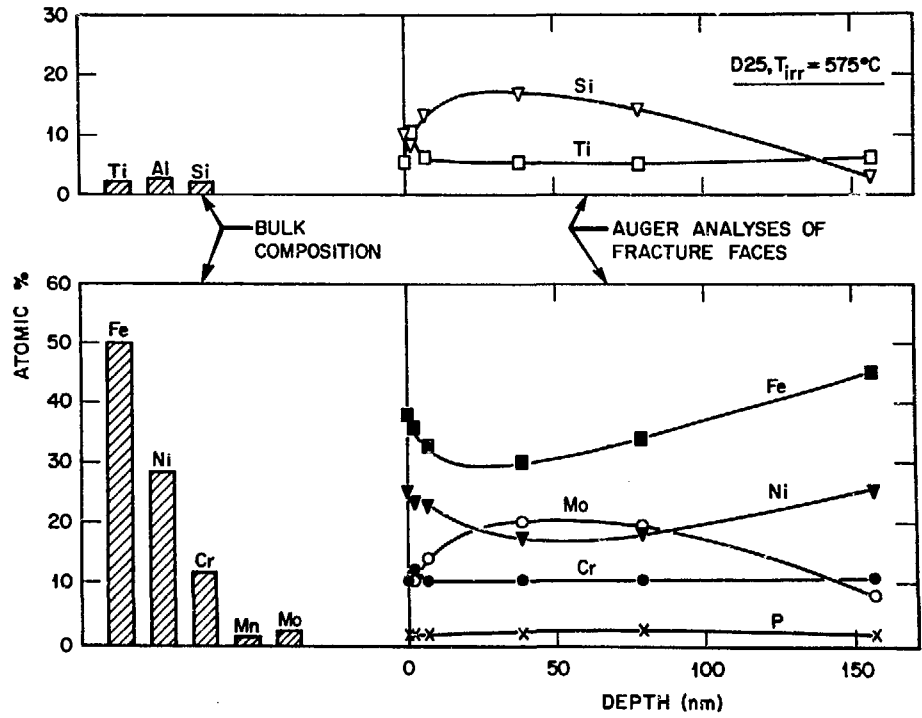


Fig. 4. D25 Alloy. Bulk composition and AES analyses of intergranular fracture surfaces.

ORNL PHOTO 1730-86

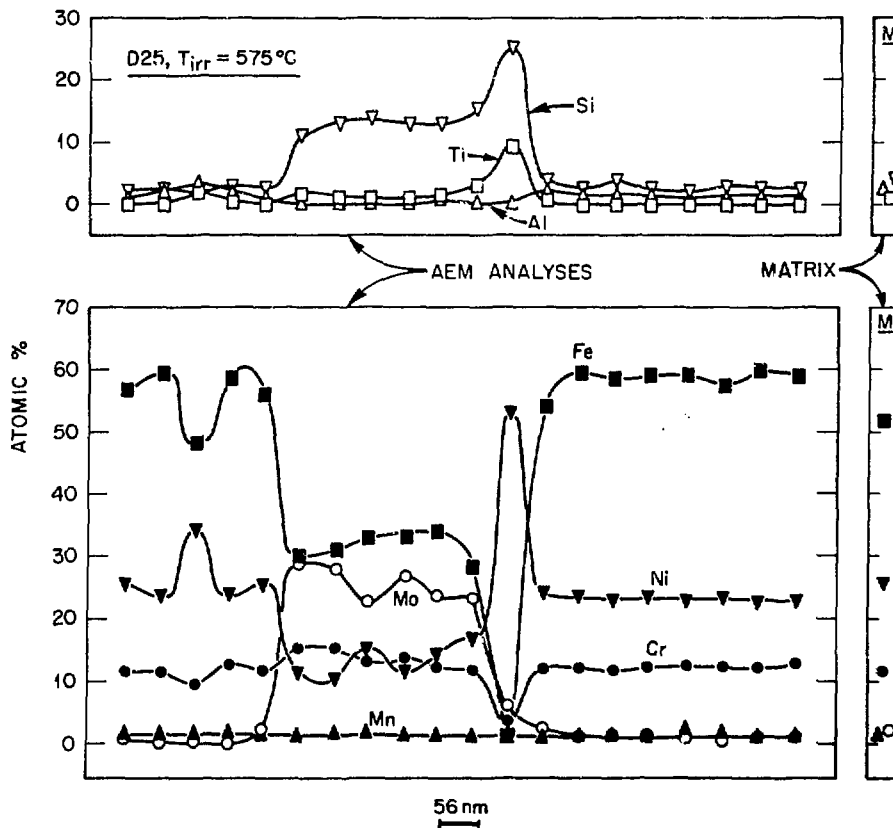


Fig. 5. D25 Alloy. AEM composition data measured across precipitate phases on a grain boundary.